Large magnetic gap at the Dirac point in a Mn-induced Bi$_2$Te$_3$ heterostructure

E. D. L. Rienks[1,2,3,*], S. Wimmer[4,*], P. S. Mandal[1,5], O. Caha[6], J. Růžička[6], A. Ney[4], H. Steiner[4], V. V. Volobuev[4,7,8], H. Groiss[9], M. Albu[10], S. A. Khan[11], J. Minár[11], H. Ebert[12], G. Bauer[4], A. Varykhalov[1], J. Sánchez-Barriga[1], O. Rader[1], G. Springholz[4]

[1]*Helmholtz-Zentrum Berlin für Materialien und Energie, Elektronenspeicherring BESSY II, Albert-Einstein-Straße 15, 12489 Berlin, Germany*

[2] *Institut für Festkörperphysik, Technische Universität Dresden, 01062 Dresden, Germany*

[3] *Leibniz-Institut für Festkörper- und Werkstofforschung Dresden, Helmholtzstraße 20, 01069 Dresden, Germany*

[4]*Institut für Halbleiter- und Festörperphysik, Johannes Kepler Universität, Altenberger Straße 69, 4040 Linz, Austria*

[5]*Institut für Physik und Astronomie, Universität Potsdam, Karl-Liebknecht-Straße 24/25, 14476 Potsdam, Germany*

[6] *Department of Condensed Matter Physics, Masaryk University, Kotlářská 267/2, 61137 Brno, Czech Republic*

[7] *National Technical University "Kharkiv Polytechnic Institute", Frunze Street 21, 61002 Kharkiv, Ukraine*

[8] *Institute of Physics, Polish Academy of Sciences, Al. Lotnikow 32/46, 02-668 Warsaw, Poland*

[9] *Zentrum für Oberflächen- und Nanoanalytik, Johannes Kepler Universität, Linz, 4040 Linz, Austria*

[10] *Graz Center for Electron Microscopy, Steyrergasse 17, 8010 Graz, Austria*

[11] *New Technologies Research Centre, University of West Bohemia, Univerzitni 8, 306 14 Pilsen, Czech Republic and*

[12] *Department Chemie, Ludwig-Maximilians-Universität München, Butenandtstr. 5-13, 81377 München, Germany*

Abstract

Magnetically doped topological insulators enable the quantum anomalous Hall effect (QAHE) which provides quantized edge states for lossless charge transport applications [1–9]. The edge states are hosted by a magnetic energy gap at the Dirac point [2] but all attempts to observe it directly have been unsuccessful. The size of this gap is considered the clue to overcoming the present limitations of the QAHE, which so far occurs only at temperatures one to two orders of magnitude below its principle limit set by the ferromagnetic Curie temperature T_C [8, 9]. Here, we use low temperature photoelectron spectroscopy to unambiguously reveal the magnetic gap of Mn-doped Bi_2Te_3 films which is present only below T_C. Surprisingly, the gap turns out to be ~ 90 meV wide, which not only exceeds $k_\mathrm{B}T$ at room temperature but is also 5 times larger than predicted by density functional theory [10]. By an exhaustive multiscale structure characterization we show that this enhancement is due to a remarkable structure modification induced by Mn doping. Instead of a disordered impurity system, it forms an alternating sequence of septuple and quintuple layer blocks, where Mn is predominantly incorporated in the center of the septuple layers. This self-organized heterostructure substantially enhances the wave-function overlap and the size of the magnetic gap at the Dirac point, as recently predicted [11]. Mn-doped Bi_2Se_3 forms a similar heterostructure, however, only a large, albeit nonmagnetic gap is formed. We explain both differences based on the higher spin-orbit interaction in Bi_2Te_3 with the most important consequence of a magnetic anisotropy perpendicular to the films, whereas for Bi_2Se_3 the spin-orbit interaction it is too weak to overcome the dipole-dipole interaction. Our findings provide crucial insights for pushing the lossless transport properties of topological insulators towards room-temperature applications.

The quantum anomalous Hall effect (QAHE) is characterized by a quantized Hall resistance $\rho_{xy} = h/(Ne^2)$ where N is an integer number N of gapless 1D edge states and which does not require the presence of an external magnetic field [1, 2]. Magnetically doped 3D topological insulators of the tetradymite family [2] have led to the first demonstration of the QAHE in Cr-doped $(Bi, Sb)_2Te_3$ [3–7]. Later on, the replacement of Cr by V as magnetic dopant delivered the first precise quantized values for ρ_{xy} as well as a vanishing ρ_{xx} at zero magnetic field [8, 9], which is the key signature for lossless charge transport through edge channel devices [12]. A crucial issue which would help to understand and develop the QAHE further towards applications has, however, remained fundamentally open – the observation and quantification of the magnetic gap at the Dirac point [2].

In a magnetic topological insulator the QAHE occurs due to a modification of the band inversion, in which at the onset of ferromagnetic order the inversion of one of the spin subbands is released by the exchange splitting and spin orbit coupling [2]. The observation of this exchange splitting has, however, remained elusive. It manifests itself as a magnetic gap at the Dirac point that opens when the system is cooled below the ferromagnetic transition temperature. The size of the gap is the crucial parameter for the temperature at which the QAHE can be observed. So far, this temperature is very low, typically around 50 mK [9] to 2 K [13, 14], which is one to two orders of magnitude lower than the ferromagnetic T_C of these systems. First principles calculations have recently suggested that the magnetic gap can be enhanced in topological insulator heterostructures [11].

Angle resolved photoemission spectroscopy (ARPES) is the method of choice for the direct observation of the magnetic gap and the verification of these predictions. Nevertheless, the experimental situation appears confusing: Large gaps at the Dirac point of the order of 0.1–0.2 eV of Bi_2Se_3 doped with Mn [15, 16] were explicitly shown to be *not* of magnetic origin [16]. On the contrary, no gaps are observed for Bi_2Se_3 when magnetic impurities are deposited directly on its surface [16–19]. Also, no gap appears when Mn is doped in the bulk of Bi_2Te_3 where the Dirac cone was found to remain intact at temperatures down to 12 K [20]. For V-doped Sb_2Te_3 a mobility gap of 32 meV was inferred from scanning tunneling Landau level spectroscopy at 1.3 K in comparison to pure Sb_2Te_3 [21], but due to the strong overlap with magnetic impurity states, no gap could be observed in the local density of states and no correlation to magnetism was reported. For Cr-doped $(Bi, Sb)_2Te_3$ an average gap of 56 meV was found by tunneling spectroscopy [22], but again its origin

remained elusive because no temperature dependence was found. In fact, a gap as large as $\sim$75 meV was found for Bi_2Se_3 with 4% Cr by ARPES *even at room temperature* [23]. This clearly suggests a non-magnetic origin of these effects because the ferromagnetic T_C is well below 50 K in all of these systems.

Interestingly, also the nature of the magnetic doping has remained under debate. For isovalent doping, it was predicted that Bi_2Se_3, Bi_2Te_3 and Sb_2Te_3 will form a QAHE state. Thus, this should occur for doping with Cr or Fe but not for Ti or V [2]. The fact that so far, V-doped $(Sb,Bi)_2Te_3$ displays the highest QAHE temperatures shows that the situation is more complex. In particular, non-isovalent magnetic dopants turn out to surprisingly little affect the Fermi level and carrier concentration. For example, Mn-doped Bi_2Se_3 and Bi_2Te_3 always remain n-type [16, 20] despite the fact that divalent Mn replacing trivalent Bi should act as a strong acceptor. These puzzling issues are related to the comparatively complex tetradymite lattice structure consisting of quintuple layers separated by van der Waals gaps and the distribution of the dopants over a large number of electrically and magnetically inequivalent incorporation sites offered by the huge tetradymite unit cell consisting of thirty individual atoms. Hence, the actual magnetic dopant distribution is a key for understanding their impact on magnetism and band topology of the system.

To resolve these issues, we present here a comprehensive study of Mn-doped Bi_2Te_3 and Bi_2Se_3 films grown under nearly identical conditions. Our data unequivocally reveals a pronounced magnetic exchange splitting at the Dirac point in Bi_2Te_3, by far exceeding previous theoretical calculations [10]. It vanishes above the ferromagnetic Curie temperature, being clear cut evidence for its magnetic origin. On the other hand, no such gap could be identified for Mn-doped Bi_2Se_3 even at 1 K. By multiscale characterization, we find that the actual lattice structure is very different from the anticipated random impurity system: Mn doping induces the formation of self-organized heterostructures consisting of stacked quintuple and septuple layers. This turns out to be very efficient for obtaining large magnetic gaps. As further crucial factors that distinguish the telluride and selenide systems, we identify the spin-orbit interaction and the way the heterostructures evolve with the Mn concentration.

Temperature-dependent band gap and magnetism

Figure 1 shows for Mn-doped Bi_2Te_3 and Bi_2Se_3 ARPES dispersions of the Dirac cone measured above and below the ferromagnetic phase transition (T_C = 10 and 6 K, respectively)

for the same 6% Mn concentration. For Mn-doped Bi_2Te_3, the photoemission spectrum from the center of the surface Brillouin zone shows an intensity maximum due to bulk transitions (50 eV photon energy), while the Dirac point (E_D) of the surface state contributes a smaller peak at ~0.3 eV binding energy. Upon cooling of the sample from 20 K through T_C down to 1 K, the low-binding energy flank of the peak develops a pronounced shoulder, forming a plateau around 0.2 eV, as can be seen in Fig. 1(a–c). We have quantified this change by linear fits to small sections of the spectrum, indicated in Fig. 1(c), with the condition that the slopes at 20 and 1 K are the same. The obtained shifts (S1 ~ 21 meV > S2 ~ 12 meV) are compatible with the scenario in which a single component for the topological surface state at 20 K is split into two equally intense components at 1 K. A simulation of this scenario (Fig. 1(d)) shows that, for a reasonable parameter range, the gap that opens at the Dirac point is 2.5–3 times larger than the sum of shifts (S1 + S2). We therefore arrive at an estimate of the gap Δ of 90 ± 10 meV at low temperature. Because the ferromagnetic T_C amounts to ~10 K in this sample, this is the clear and unambiguous proof of the magnetic origin of this gap. This is the central result of the present work.

What is probed by the gap at the Dirac point is the exchange splitting of p-electrons of the Bi_2Te_3 host material which ferromagnetically couple the localized magnetic moments of the Mn ions [10]. The magnitude of the gap at the Dirac point depends on the exchange coupling J and the magnetization along the [0001] surface normal [24]. This behavior is principally similar to that of the magnetic gap of Mn-doped multiferroic GeTe [25] (although that system is of Rashba type and topologically trivial). Returning to Fig. 1, we see that this criterion is *not* fulfilled for Mn-doped Bi_2Se_3 with 6% Mn, where we find a large gap at the Dirac point of ~200 meV at all temperatures from 1 to 300 K [16]. The gap size does not increase when we cool down to 1 K, i.e., well below $T_C \sim 6$ K. This rules out a significant contribution of magnetism to the Dirac cone gap in Mn-doped Bi_2Se_3, contrary to the case of Bi_2Te_3, and serves as an additional cross-check for the magnetic gap opening.

Figure 2 shows magnetization measurements for Mn-doped Bi_2Te_3 and Bi_2Se_3 samples with comparable Mn concentrations. The Bi_2Te_3 sample shows an easy axis magnetization **M** along the c axis normal to the surface, i.e., $M_\perp > M_\parallel$. This perpendicular anisotropy is robust since it does not depend on the Mn concentration (see Supplementary Information) and is observed also for bulk single crystals [26, 27]. In contrast, for Mn-doped Bi_2Se_3 the easy axis is parallel to the surface plane – also stable in a large concentration range (see

Supplementary Information). This opposite behavior is also revealed by magnetotransport measurements shown in Fig. 2(c,d), where with magnetic fields applied perpendicular to the films only Mn-doped Bi_2Te_3 displays a pronounced anomalous Hall effect (AHE) upon cooling below T_C whereas it is negligible in Bi_2Se_3 (Fig. 2(d)).

While an in-plane magnetization merely shifts the Dirac cone in momentum space parallel to the surface [10, 28], the perpendicular anisotropy in Mn-doped Bi_2Te_3 is precisely the precondition for the magnetic band gap opening and for the QAHE. Density functional theory (DFT) has predicted the resulting magnetic Dirac gap as 16 meV for 10% Mn substitutionally incorporated in the topmost quintuple layer of Bi_2Te_3 [10], but this gap has so far not been experimentally demonstrated. More astonishingly, the magnetic gap of 90 ± 10 meV that we observe is 5× as large as the theoretical prediction.

To resolve this discrepancy, we return to Fig. 2, where besides the obvious difference in magnetic anisotropy, there are a several other interesting differences between the two systems: Firstly, the coercive field of Mn-doped Bi_2Te_3 is significantly larger than for Bi_2Se_3, which only shows a very narrow opening of the hysteresis loop. Secondly, at the same time the anisotropy field, at which in-plane and out-of-plane magnetizations are equal is two times higher for Bi_2Te_3 (see Supplementary Information). Finally, the ferromagnetic T_C of Mn-doped Bi_2Te_3 is considerably larger (7–15 K) than for Bi_2Se_3 (5–7 K) (see inserts in Fig. 2(a,b)) and depends more strongly on the Mn concentration. Altogether this demonstrates that Mn-doped Bi_2Te_3 is the more robust and anisotropic ferromagnet.

Multiscale structure analysis

To clarify how Mn is actually incorporated in Bi_2Te_3 and Bi_2Se_3 a systematic multiscale structure analysis was performed for both types of samples. Figure 3(a) shows Mn-doped Bi_2Te_3 in high-resolution scanning transmission electron microscopy (HRSTEM), measured along the $[\bar{1}100]$ direction for 10% Mn. Strikingly, we observe upon Mn doping instead of the expected periodic sequence of Te-Bi-Te-Bi-Te quintuple layers the emergence of a novel structure consisting of septuple and quintuple layers that does not exist for stoichiometric Bi_2Te_3. The septuple layers consist of the sequence Te-Bi-Te-Mn-Te-Bi-Te, where the Mn atoms occupy the central septuple atomic layer as found in Bi_2MnTe_4 crystals [29]. This self-organized heterostructure formation obviously disagrees with the common notion of substitutional Mn incorporation in Bi_2Te_3 assumed in most previous studies [10, 26, 30].

Mn is not isoeletronic to Bi due to the different number of valence electrons. Therefore, substitutional Mn on Bi sites should be a strong acceptor inducing a strong p-type doping of the system. This is neither observed for Mn-doped Bi_2Te_3 nor Bi_2Se_3 which always remain n-type even at high Mn concentrations [16, 20, 27, 31]. On the other hand, Mn incorporated in Bi_2MnTe_4 septuple layers is not electrically active because the septuple is formed by addition of a charge compensated MnTe double layer to a quintuple layer. Apart from compensation effects, this explains the surprisingly small effect of Mn-doping on carrier concentration and Fermi level of the system. According to Fig. 3(b), the formation of Mn-induced septuple/quintuple heterostructures also occurs in Bi_2Se_3 and the formation of septuple layers was also recently seen for Mn-doped Bi_2Se_3 films [32].

To obtain element specific information on the Mn incorporation sites, x-ray absorption near-edge spectroscopy (XANES) and extended x-ray absorption fine structure spectroscopy (EXAFS) were performed at the MnK-edge as summarized in Fig. 4. The absorption spectra were analyzed by simulations for all possible Mn incorporation sites, ranging from Mn in the center of the Bi_2MnTe_4 (Bi_2MnSe_4) septuple layers, substitutional Mn on Bi sites in the quintuple layers, interstitial Mn in the van der Waals gap in either octahedral or tetrahedral coordination (see Fig. 4(e–g)). In addition, we considered also Mn on anion Te (Se) antisites i.e., on Te1 (and Se1) sites at the outer layers and on Te2 (and Se2) sites in the center of the quintuple layers. Contrary to most theoretical investigations based on substitutional Mn incorporation [10], our analysis shows that Mn in Bi_2Te_3 prefers to be incorporated in septuple layers and only a minority as substitutional Mn in the quintuple layers. While the EXAFS data does not rule out Mn on octrahedral sites in the van der Waals gap, the fact that septuples are never seen in undoped Bi_2Te_3 clearly suggests that the Mn sites are closely linked to the septuple layers.

Turning to Mn-doped Bi_2Se_3 shown in Figs. 4(b,d), we do not observe as intense EXAFS oscillations as for Bi_2Te_3. This indicates stronger cancellation effects caused by Mn distributed over different lattice sites, including a larger amount of substitutional Mn and a lesser fraction within the septuple layers. This is highlighted by the XANES spectra at the MnK-edge which exhibit a characteristic double peak structure at higher and lower photon energy, attributed respectively to Mn in the center of the septuple and to substitutional Mn in the quintuple layers, where again for Bi_2Se_3 the signal from Mn in the septuple layers is weaker as compared to Mn in Bi_2Te_3. For tetrahedrally coordinated interstitial Mn, as well

as for Mn on Te (Se) antisites, the simulations do not agree with the experiments, indicating that these are not favorable for Mn incorporation. Overall, we conclude that for Bi_2Te_3 the vast majority of Mn is incorporated within the septuple layers and that substitutional Mn is more readily formed in Bi_2Se_3, especially at lower Mn concentrations, with an overall broader distribution of Mn over various other lattice sites.

Our results so far suggest a unique heterostructure formation upon Mn-doping but the HRSTEM, XANES, and EXAFS data deliver only a local picture. To systematically characterize its evolution on a larger length scale and its dependence on the Mn concentration, x-ray diffraction investigations were performed as summarized in Fig. 5. For both systems we indeed find a pronounced change of the diffraction spectra with increasing Mn content. This is evidenced by the appearance of additional diffraction peaks (see Fig. 5(a,b)) that signify the emergence of septuple layers in the structure. However, the substantial broadening of the peaks reveal that the septuple layers are not incorporated periodically at fixed distances, but rather stochastically after a varying number N_{QL} of quintuple layers as seen in the STEM cross-sections where N_{QL} varies between one to seven. This requires us to develop a one-dimensional paracrystal model to describe and evaluate the experimental diffraction data, as detailed in the Supplementary Information. In this model, the overall structure is described as a statistically varying sequence of quintuple segments alternating with single septuple layers that is characterized by the average number $\langle N_{\mathrm{QL}} \rangle$ between subsequent septuples and by the randomness of the statistical distribution of the N_{QL}, i.e., their root mean square (RMS) deviation from the average value.

The model fits displayed by the black lines in Figs. 5(a,b) show a remarkably good agreement with the diffraction spectra for all Mn concentrations. This impressively corroborates the formation of self-organized quintuple/septuple layer heterostructures in both the Bi_2Te_3 and Bi_2Se_3 systems. From the fits, the average $\langle N_{\mathrm{QL}} \rangle$ between the septuple layers (and, thus, the density of septuple layers) as a function of Mn content is obtained, which is displayed in Fig. 5(c) together with the statistical variation of N_{QL}. Apparently, in Bi_2Te_3 the formation of septuple layers starts at lower Mn concentration and the average separation between the septuple layers is substantially smaller than in Bi_2Se_3. This evidences the higher probability of septuple layer formation for Bi_2Te_3, in agreement with the XANES and EXAFS result. This difference is further highlighted by Fig. 5(d), where the derived number of available Mn sites in the septuples is plotted versus the actual Mn concentration, revealing that in Bi_2Te_3

all Mn atoms can be incorporated in the septuple layers, whereas in Bi_2Se_3 the density of septuple layers at low Mn concentrations is too small to accommodate all Mn atoms, i.e., a significant Mn fraction must be incorporated on other sites as well.

Discussion

The electronic structure of transition metal impurities at the surface and in the bulk of Bi_2Te_3 and Bi_2Se_3 has been studied extensively by density functional theory (DFT) calculations. A magnetic band gap of ∼10 meV has been predicted for Co-doped Bi_2Se_3 [30] and of 16 meV for Mn-doped Bi_2Te_3 [10]. By the splitting of the Dirac point we probe the exchange interaction at the Te sites. This has been confirmed by DFT, where the spectral density of the split Dirac point is nine times more strongly localized at the Te atoms than at the other sites [10]. The calculated gap value of 16 meV for substitutionally Mn-doped Bi_2Te_3 by Henk et al. [10] for a Mn concentration of 10% is, however, substantially smaller that the magnetic gap of 90 meV revealed by our experiments. For Mn in Bi_2Se_3, a nonmagnetic band gap of the measured size (∼200 meV) does not appear in any DFT calculation. At least, DFT reveals in principle that, depending on orbital symmetry, small gaps in the Dirac cone may open due to hybridization with transition metal impurity states. Accordingly, a hybridization gap of ∼ 4 meV at the Dirac point was suggested for substitutional Mn in Bi_2Se_3 for an in-plane (*sic!*) magnetization [33], which is obviously much less than what we experimentally observe. The only prediction of a such a nonmagnetic gap which also has the magnitude seen in our experiments is from calculations assuming an on-site Coulomb interaction U at the impurity site [34].

The structural information gained in the present study helps to clarify the question of the origin of this nonmagnetic gap: Apparently, Mn forms more substitutional sites in Bi_2Se_3 than in Bi_2Te_3 where Mn is preferentially incorporated into septuple layers. Mn in the substitutional site will lead to a larger Coulomb U than in the central Mn monolayer of the septuple layer, where Mn $3d$ levels can delocalize in the plane. We could recently demonstrate experimentally that U, termed previously as impurity strength [34], indeed influences the size of the nonmagnetic gap strongly. For example, indium impurities are known to enhance the spacing across which surface-surface coupling opens a gap at the Dirac point [35]. When we compare Mn doping with In doping in Bi_2Se_3, we find that to reach the same gap size as for 8% Mn, only 2% In is required [16, 36]. However, the effect of

impurities on the nonmagnetic gap decreases with higher spin-orbit interaction of the host material as shown by our recent work [36]. Thus, Bi_2Te_3 is principally less susceptible to opening of a nonmagnetic gap than Bi_2Se_3, regardless of the structural differences induced by Mn doping.

To explain the marked difference in the magnetic anisotropy of Mn-doped Bi_2Te_3 and Bi_2Se_3 including the structural motif of the septuple layers, we compute the magnetic anisotropy using ab initio calculations (see Supplementary Information) for unit cells consisting of one Bi_2MnX_4 septuple layer and one Bi_2X_3 quintuple layer (X=Te, Se). We find that the magnetocrystalline anisotropy inducing the out-of-plane spin orientation is 3.5 times larger in the telluride than in the selenide system. This is due to the higher spin-orbit interaction in Bi_2Te_3 and is related to warping effects in the Dirac cone, which turn the spins out of the plane [37]. The magnetocrystalline anisotropy is counteracted by the dipole-dipole interaction (shape anisotropy) that tends to align the magnetic moments in the plane. The shape anisotropy comes out to be very similar for the two heterostructure systems, but essentially cancels the magnetocrystalline anisotropy in Bi_2Se_3, whereas it is superseded by the magnetocrystalline anisotropy in Bi_2Te_3. Thus, the out-of-plane anisotropy persists and is nearly one order of magnitude larger than for the selenide system, where the anisotropy energy almost changes sign towards in-plane magnetization. In the real samples, the in-plane magnetization for the selenide structures may be additionally supported by the Mn atoms on substitutional sites which favor the magnetic moments to be in plane [33]. For the telluride system, the preferred perpendicular magnetization agrees well with recent model calculations by Otrokov et al. [11] who considered similar types of Bi_2MnTe_4/Bi_2Te_3 heterostructures in different septuple and quintuple combinations. We conclude that the higher spin-orbit interaction in the telluride system thus overcomes the dipole-dipole interaction and enables the formation of the magnetic gap at the Dirac point.

Finally, as mentioned above, our measured magnetic gap size of 90 meV for Mn-doped Bi_2Te_3 is five times as large as predicted for substitutional Mn incorporation (16 meV) [10]. This represents a huge enhancement that is obviously related to the naturally formed quintuple/septuple layer heterostructures. As pointed out by Otrokov et al. [11] the Mn monolayer in the center of Bi_2MnTe_4 septuples enhances the wave function overlap strongly, supporting magnetic gaps as high as $38 - 87$ meV, depending on the chosen Bi_2MnTe_4/Bi_2Te_3 combination. This is in excellent agreement with the enhancement found in our experiments.

This demonstrates the great potential of such structures for stabilizing edge transport in QAHE devices. Theory [11] also suggest that the nontrivial topology is retained, by the calculation of the Chern number $C = -1$ for the heterostructure system, consisting of one Bi_2MnTe_4 septuple and two Bi_2Te_3 quintuple layers, and by the persistence of the Dirac cone surface state. This is confirmed by our ARPES measurements above and below T_C.

In conclusion, we have demonstrated unambiguously and for the first time the opening of a magnetic gap in a topological insulator below the ferromagnetic phase transition and its closure for $T > T_C$. The magnetic gap in Mn-doped Bi_2Te_3 is remarkably large (90±10 meV) as a result of the formation of a natural heterostructure in which Mn is incorporated within septuple layers instead of simple substitutional incorporation. Our results thus support recent theoretical predictions that magnetic gaps in topological insulators can be significantly enhanced in multi-layered systems [11]. These are considered as a basis for the realization of new topological phases such as the axion insulator state exhibiting quantized magnetoelectric effects [14, 38] and the chiral Majorana fermion [39]. No magnetic gap is detected for Mn-doped Bi_2Se_3 within the experimental resolution but instead, a very large non-magnetic gap that does not increase even when cooling down to 1 K, well below T_C, and thus does not have a magnetic contribution. We correlate this with the difference in magnetic anisotropy due to the much larger spin-orbit interaction in Bi_2Te_3 and offer a unifed picture for both observations. Returning to the question of enhanced QAHE devices, up to now the focus has been on increasing the Curie temperatures of the systems, e.g., by obtaining a high density of st ates at the Fermi level to increase the exchange integrals. Instead, the magnetic gap size may turn out to be the more decisive factor for pushing up the operation temperature. Due to the large magnetic gap size, Mn-doping seems to be most promising in this respect and will open up new perspectives for device realization.

Data availability

The data sets generated and analysed during the current study are available from the corresponding authors on reasonable request.

Code availability

The code for the paracrystal model is available from the corresponding authors upon request. The employed electronic structure codes Wien2K and SPR-KKR and x-ray absorption fine

structure codes FDMNES and FEFF9 can be downloaded after the corresponding licence requirements given on the respective webpages are fulfilled.

Corresponding authors: G. Springholz, email: gunther.springholz@jku.at, O. Rader, email: rader@helmholtz-berlin.de.

* These authors contributed equally to the present work.

---

[1] M. Onoda, N. Nagaosa, Quantized Anomalous Hall Effect in Two-Dimensional Ferromagnets: Quantum Hall Effect in Metals, Phys. Rev. Lett. 90, 206601 (2003).

[2] R. Yu et al., Quantized anomalous Hall effect in magnetic topological insulators, Science 329, 61 (2010).

[3] C.-Z. Chang et al., Experimental observation of the quantum anomalous Hall effect in a magnetic topological insulator, Science 340, 167 (2013).

[4] J. G. Checkelsky, R. Yoshimi, A. Tsukazaki, K. S. Takahashi, Y. Kozuka, J. Falson, M. Kawasaki, Y. Tokura, Trajectory of the anomalous Hall effect toward the quantized state in a ferromagnetic topological insulator, Nature Phys. 10, 731 (2014).

[5] X. Kou, S.-T. Guo, Y. Fan, L. Pan, M. Lang, Y. Jiang, Q. Shao, T. Nie, K. Murata, J. Tang, Y. Wang, L. He, T.-K. Lee, W.-L. Lee, K. L. Wang, Scale-Invariant Quantum Anomalous Hall Effect in Magnetic Topological Insulators beyond the Two-Dimensional Limit, Phys.

Rev. Lett. 113, 137201 (2014).

[6] A. J. Bestwick, E. J. Fox, X. Kou, L. Pan, K. L. Wang, D. Goldhaber-Gordon, Precise Quantization of the Anomalous Hall Effect near Zero Magnetic Field, Phys. Rev. Lett. 114, 187201 (2015).

[7] Abhinav Kandala, Anthony Richardella, Susan Kempinger, Chao-Xing Liu, and Nitin Samarth, Giant anisotropic magnetoresistance in a quantum anomalous Hall insulator, Nature Commun. 6, 7434 (2015).

[8] C.-Z. Chang, W. Zhao, D. Y. Kim, H. Zhang, B. A. Assaf, D. Heiman, S.-C. Zhang, C. Liu, M. H. W. Chan, J. S. Moodera, High-precision realization of robust quantum anomalous Hall state in a hard ferromagnetic topological insulator, Nat. Mater. 14, 473 (2015).

[9] S. Grauer, S. Schreyeck, M. Winnerlein, K. Brunner, C. Gould, L. W. Molenkamp, Coincidence of superparamagnetism and perfect quantization in the quantum anomalous Hall state, Phys. Rev. B 92, 201304(R) (2015).

[10] J. Henk, M. Flieger, I. V. Maznichenko, I. Mertig, A. Ernst, S. V. Eremeev, E. V. Chulkov, Topological Character and Magnetism of the Dirac State in Mn-Doped Bi_2Te_3, Phys. Rev. Lett. 109, 076801 (2012).

[11] M. M. Otrokov, T. V. Menshchikova, M. G. Vergniory, I. P. Rusinov, A. Yu. Vyazovskaya, Yu. M. Koroteev, G. Bihlmayer, A. Ernst, P. M. Echenique, A. Arnau, E. V. Chulkov, Highly-ordered wide bandgap materials for quantized anomalous Hall and magnetoelectric effects, 2D Mater. 4, 025082 (2017).

[12] X. Zhang and S.-C. Zhang, Chiral interconnects based on topological insulators, Proc. SPIE Int. Soc. Opt. Eng. 8373, 837309 (2012).

[13] M. Mogi, R. Yoshimi, A. Tsukazaki, K. Yasuda, Y. Kozuka, K. S. Takahashi, M. Kawasaki, Y. Tokura, Magnetic modulation doping in topological insulators toward higher-temperature quantum anomalous Hall effect, Appl. Phys. Lett. 107, 182401 (2015).

[14] Di Xiao, Jue Jiang, Jae-Ho Shin, Wenbo Wang, Fei Wang, Yi-Fan Zhao, Chaoxing Liu, Weida Wu, Moses H.W. Chan, Nitin Samarth, and Cui-Zu Chang, Realization of the Axion Insulator State in Quantum Anomalous Hall Sandwich Heterostructures, Phys. Rev. Lett. 120, 056801 (2018).

[15] D. Zhang, A. Richardella, D. W. Rench, S.-Y. Xu, A. Kandala, T. C. Flanagan, H. Beidenkopf, A. L. Yeats, B. B. Buckley, P. V. Klimov, D. D. Awschalom, A. Yazdani, P. Schiffer,

M. Z. Hasan, N. Samarth, Interplay between ferromagnetism, surface states, and quantum corrections in a magnetically doped topological insulator, Phys. Rev. B 86, 205127 (2012).

[16] J. Sánchez-Barriga, A. Varykhalov, G. Springholz, H. Steiner, R. Kirchschlager, G. Bauer, O. Caha, E. Schierle, E. Weschke, A. A. Ünal, S. Valencia, M. Dunst, J. Braun, H. Ebert, J. Minár, E. Golias, L. V. Yashina, A. Ney, V. Holý, O. Rader, Nonmagnetic band gap at the Dirac point of the magnetic topological insulator $(Bi_{1-x}Mn_x)_2Se_3$, Nat. Commun. 7, 10559 (2016).

[17] T. Valla, Z.-H. Pan, D. Gardner, Y. S. Lee, S. Chu, Photoemission Spectroscopy of magnetic and nonmagnetic impurities on the surface of the Bi_2Se_3 topological insulator, Phys. Rev. Lett. 108, 117601 (2012).

[18] M. R. Scholz, J. Sánchez-Barriga, D. Marchenko, A. Varykhalov, A. Volykhov, L. V. Yashina, O. Rader, Tolerance of Topological Surface States towards Magnetic Moments: Fe on Bi_2Se_3, Phys. Rev. Lett. 108, 256810 (2012).

[19] J. Honolka, A. A. Khajetoorians, V. Sessi, T. O. Wehling, S. Stepanow, J.-L. Mi, B. B. Iversen, T. Schlenk, J. Wiebe, N. B. Brookes, A. I. Lichtenstein, Ph. Hofmann, K. Kern, R. Wiesendanger, In-Plane Magnetic Anisotropy of Fe Atoms on Bi_2Se_3(111), Phys. Rev. Lett. 108, 256811 (2012).

[20] J. Ružička, O. Caha, V. Holý, H. Steiner, A. Ney, G. Bauer, T. Duchoň, K. Veltruska, I. Khalakhan, V. Matolin, E. F. Schwier, H. Iwasawa, K. Shimada, G. Springholz, Structural and electronic properties of manganese-doped Bi_2Te_3 epitaxial layers, New J. Phys. 17, 013028 (2015).

[21] P. Sessi, R. R. Biswas, T. Bathon, O. Storz, S. Wilfert, A. Barla, K. A. Kokh, O. E. Tereshchenko, K. Fauth, M. Bode, A. V. Balatsky, Dual nature of magnetic dopants and competing trends in topological insulators, Nat. Commun. 7, 12027 (2016).

[22] I. Lee, C. K. Kim, J. Lee, S. J. L. Billinge, R. Zhong, J. A. Schneeloch, T. Liu, T. Valla, J. M. Tranquada, G. Gu, J. C. S. Davis, Imaging Dirac-mass disorder from magnetic dopant atoms in the ferromagnetic topological insulator $Cr_x(Bi_{0.1}Sb_{0.9})_{2-x}Te_3$, Proc. Natl. Acad. Sci. U. S. A. 112, 1316 (2015).

[23] Cui-Zu Chang, Peizhe Tang, Yi-Lin Wang, Xiao Feng, Kang Li, Zuocheng Zhang, Yayu Wang, Li-Li Wang, Xi Chen, Chaoxing Liu, Wenhui Duan, Ke He, Xu-Cun Ma, and Qi-Kun Xue, Chemical-Potential-Dependent Gap Opening at the Dirac Surface States of Bi_2Se_3 Induced

by Aggregated Substitutional Cr Atoms, Phys. Rev. Lett. 112, 056801 (2014).

[24] G. Rosenberg, M. Franz, Surface magnetic ordering in topological insulators with bulk magnetic dopants, Phys. Rev. B 85, 195119 (2012).

[25] J. Krempaský, S. Muff, F. Bisti, M. Fanciulli, H. Volfová, A. P. Weber, N. Pilet, P. Warnicke, H. Ebert, J Braun, F. Bertran, V. V. Volobuev, J. Minár, G. Springholz, J.H. Dil, V. N. Strocov, Entanglement and manipulation of the magnetic and spinorbit order in multiferroic Rashba semiconductors, Nat. Commun. 7, 13071 (2016).

[26] Y. S. Hor, P. Roushan, H. Beidenkopf, J. Seo, D. Qu, J. G. Checkelsky, L. A. Wray, D. Hsieh, Y. Xia, S.-Y. Xu, D. Qian, M. Z. Hasan, N. P. Ong, A. Yazdani, R. J. Cava, Development of ferromagnetism in the doped topological insulator $Bi_{2-x}Fe_xTe_3$, Phys. Rev. B 81, 195203 (2010).

[27] M. D. Watson, L. J. Collins-McIntyre, A. I. Coldea, D. Prabhakaran, L. R. Shelford, S. C. Speller, T. Mousavi, C. Grovenor, Z. Salman, S. R. Giblin, G. van der Laan, T. Hesjedal, Study of the structural, electric and magnetic properties of Mn-doped Bi_2Te_3 single crystals, New J. Phys. 15, 103016 (2013).

[28] M. Kharitonov, Interaction-enhanced magnetically ordered insulating state at the edge of a two-dimensional topological insulator, Phys. Rev. B 86, 165121 (2012).

[29] D. S. Lee, T. H. Kim, C.-H. Park, C.-Y. Chung, Y. S. Lim, W.-S. Seoa, H.-H. Park, Crystal structure, properties and nanostructuring of a new layered chalcogenide semiconductor, Bi_2MnTe_4, Cryst. Eng. Comm. 15, 5532 (2013).

[30] T. M. Schmidt, R. H. Miwa, A. Fazzio, Spin texture and magnetic anisotropy of Co impurities in Bi_2Se_3 topological insulators, Phys. Rev. B 84, 245418 (2011).

[31] Joon Sue Lee, A. Richardella, D. W. Rench, R. D. Fraleigh, T. C. Flanagan, J. A. Borchers, Jing Tao, N. Samarth, Ferromagnetism and spin-dependent transport in n-type Mn-doped bismuth telluride thin films, Phys. Rev. B 89, 174425 (2014).

[32] J. A. Hagmann, Xiang Li, S. Chowdhury, S.-N. Dong, S. Rouvimov, S. J. Pookpanratana, K. M. Yu, T. A. Orlova, T. B. Bolin, C. U. Segre, D. G. Seiler, C. A. Richter, Xinyu Liu, M. Dobrowolska, J. K. Furdyna, Molecular beam growth and structure of self-assembled Bi_2Se_3/Bi_2MnSe_4 multilayer heterostructures, New J. Phys. 19, 085002 (2017).

[33] L. B. Abdalla, L. Seixas, T. M. Schmidt, R. H. Miwa, A. Fazzio, Topological insulator $Bi_2Se_3(111)$ surface doped with transition metals: an ab-initio investigation, Phys. Rev. B

88, 045312 (2013).

[34] A. M. Black-Schaffer, A. V. Balatsky, Strong potential impurities on the surface of a topological insulator, Phys. Rev. B 85, 121103(R) (2012).

[35] L. Wu, M. Brahlek, R. V. Aguilar, A. V. Stier, C. M. Morris, Y. Lubashevsky, L. S. Bilbro, N. Bansal, S. Oh, N. P. Armitage, A sudden collapse in the transport lifetime across the topological phase transition in $(Bi_{1-x}In_x)_2Se$, Nature Phys. 9, 410 (2013).

[36] J. Sánchez-Barriga, I. Aguilera, D. Y. Tsukanova, P. S. Mandal, L. V. Yashina, A. M. Abakumov, A. N. Chaika, A. Varykhalov, G. Bihlmayer, S. Blügel, O. Rader (unpublished)

[37] Liang Fu, Hexagonal Warping Effects in the Surface States of the Topological Insulator Bi_2Te_3, Phys. Rev. Lett. 103, 266801 (2009)

[38] M. Mogi, M. Kawamura, A. Tsukazaki, R. Yoshimi, K. S. Takahashi, M. Kawasaki, and Y. Tokura, Tailoring tricolor structure of magnetic topological insulator for robust axion insulator, Science Advances 10, eaao1669 (2017).

[39] Q. L. He, L. Pan, A. L. Stern, E. C. Burks, Xiaoyu Che, Gen Yin Jing Wang et el. Chiral Majorana fermion modes in a quantum anomalous Hall insulator-superconductor structure, Science 357, 294 (2017).
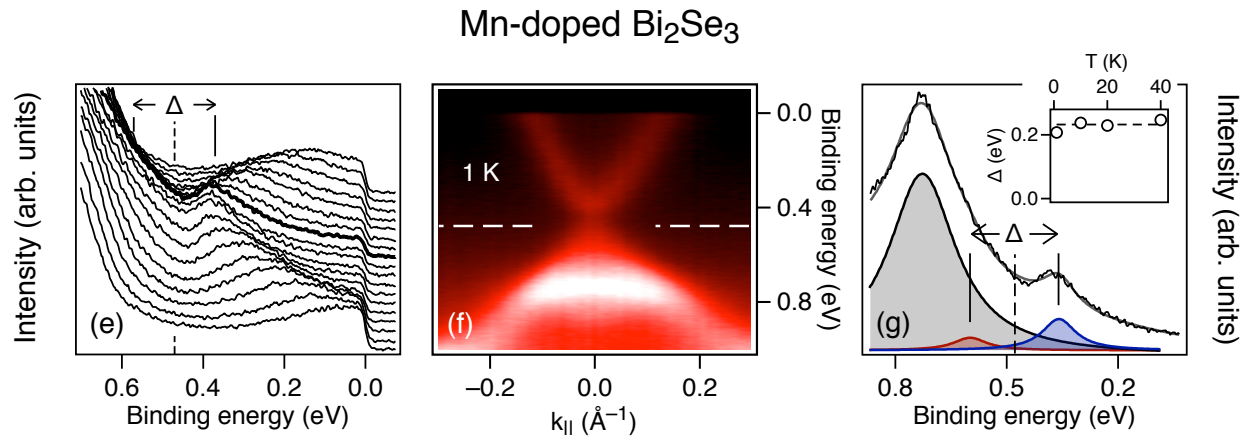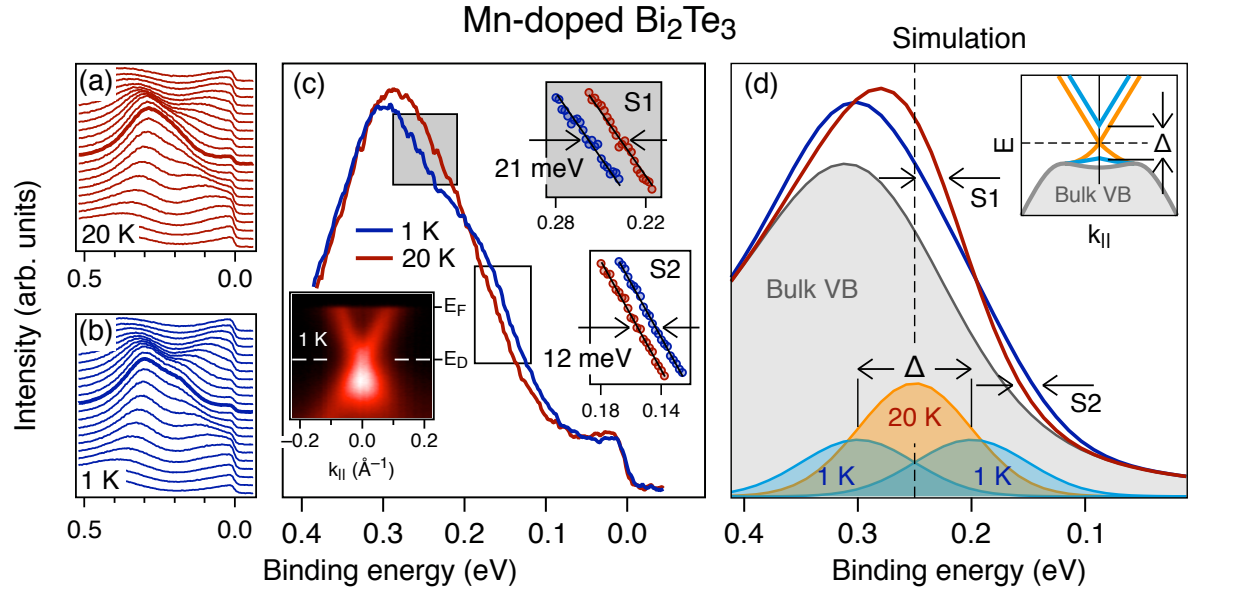
Figures

Mn-doped Bi$_2$Te$_3$

(a) 20 K

(b) 1 K

Intensity (arb. units)

0.5   0.0

0.5   0.0

(c)

S1

21 meV

0.28   0.22

1 K

E_F
E_D

1 K

−0.2   0.0   0.2

$k_{||}$ (Å^{-1})

S2

12 meV

0.18   0.14

1 K
20 K

0.4   0.3   0.2   0.1   0.0

Binding energy (eV)

Simulation

(d)

Bulk VB

S1

S2

Δ

20 K

1 K   1 K

0.4   0.3   0.2   0.1

Binding energy (eV)

E

Bulk VB

Δ

$k_{||}$

Mn-doped Bi$_2$Se$_3$

(e)

Δ

Intensity (arb. units)

0.6   0.4   0.2   0.0

Binding energy (eV)

(f)

1 K

0.0

0.4

0.8

Binding energy (eV)

−0.2   0.0   0.2

$k_{||}$ (Å^{-1})

(g)

Δ

0.8   0.5   0.2

Binding energy (eV)

Intensity (arb. units)

T (K)
0   20   40

0.2

0.0

Δ (eV)

18

FIG. 1: **Magnetic gap of Mn-doped Bi$_2$Te$_3$ derived by ARPES.** (a–d) Measurements for Bi$_2$Te$_3$ with 6% Mn performed above and below the Curie temperature $T_{\mathrm{C}} \sim 10$ K. (The spectra in (c,d,g) and those marked by thick lines in (a,b,d) correspond to the center of the surface Brillouin zone, i. e., electron wave vector component $k_\parallel = 0$ Å^{-1}.) Linear fits to the regions indicated in (c) yield shifts of 21 and 12 meV between these sections of the 20 K and 1 K spectra. (d) Simulation showing that this corresponds to a magnetic gap $\Delta = 90 \pm 10$ meV. (e–g) Same analysis for Mn-doped Bi$_2$Se$_3$ with 6% Mn and a T_{C} of 6 K, revealing only a nonmagnetic gap of 220 ± 5 meV at 20 K and 205 ± 5 meV at 1 K, determined by least-square fit to the upper Dirac cone and to the lower Dirac cone at $k_\parallel = 0$ Å^{-1}.
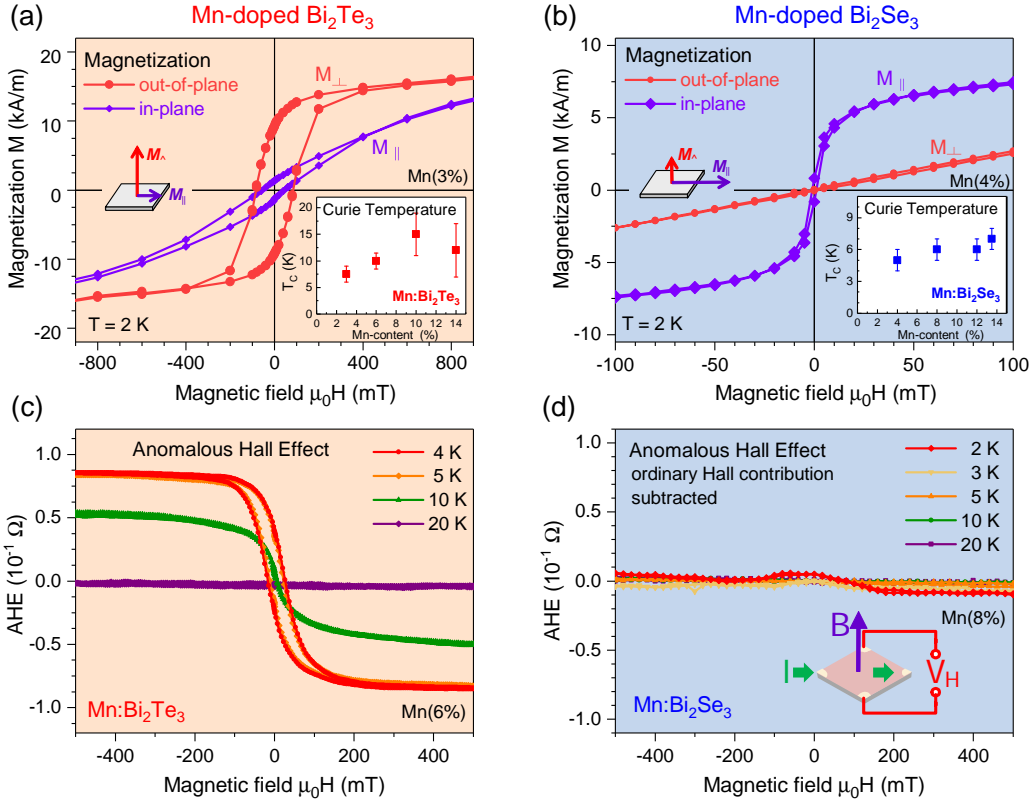
FIG. 2: **Magnetic properties.** In-plane and out-of-plane magnetization $M(H)$ of Bi_2Te_3 (a) and Bi_2Se_3 (b) films with Mn concentrations of 3 and 4 % measured at 2 K by SQUID with the magnetic field either parallel or perpendicular to the surface, evidencing a perpendicular anisotropy (easy axis) for Bi_2Te_3 and an in-plane easy axis for Bi_2Se_3. The Curie temperature as a function of Mn concentration is depicted in the inserts, evidencing that T_C is significantly higher in the telluride system. (c,d) Anomalous Hall effect (AHE) measurements of the samples with the contribution of the ordinary Hall effect extracted from the high field data subtracted (see Supplementary Information). Due to the perpendicular magnetic anisotropy, only Mn-doped Bi_2Te_3 displays a pronounced anomalous Hall effect appearing when the sample is cooled below T_C.
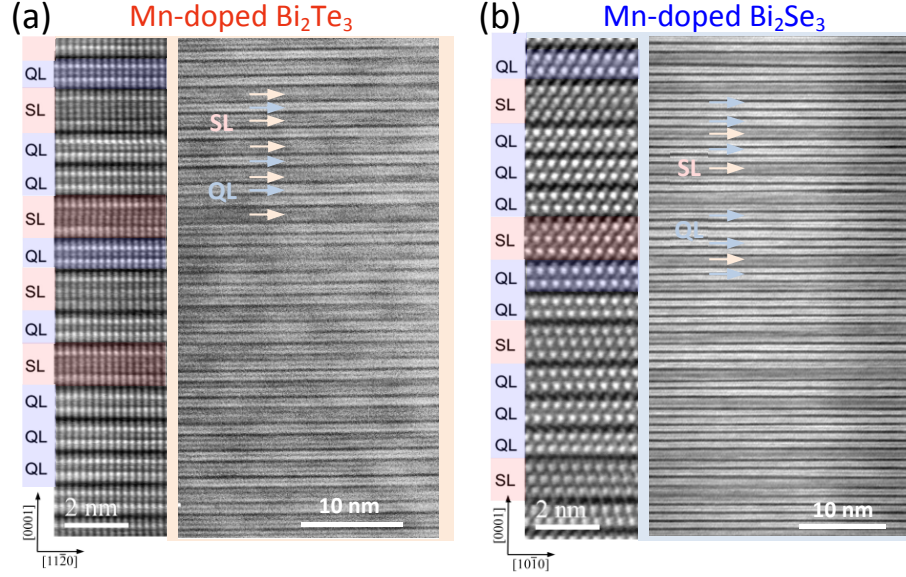
FIG. 3: **HR-STEM cross sections** of Mn-doped Bi_2Te_3 and Bi_2Se_3 recorded along the $[\bar{1}100]$ and $[\bar{1}2\bar{1}0]$ zone axis, respectively. The STEM cross sections reveal the natural formation of a layered heterostructure consisting of Bi_2MnTe_4 (Bi_2MnSe_4) septuple layers (SL) inserted between Bi_2Te_3 (Bi_2Se_3) quintuple (QL) layers adjoined by van der Waals gaps. Due to the atomic-number contrast, the heavy atoms (Bi) appear brighter in the high angle annular dark field (HAADF) images, and the septuple layers in the overview images darker due to the lighter Mn atoms preferentially incorporated. Note the different scales. The Mn concentration in (a) was 10% and in (b) locally 9% and on average 6% according to x-ray diffraction.
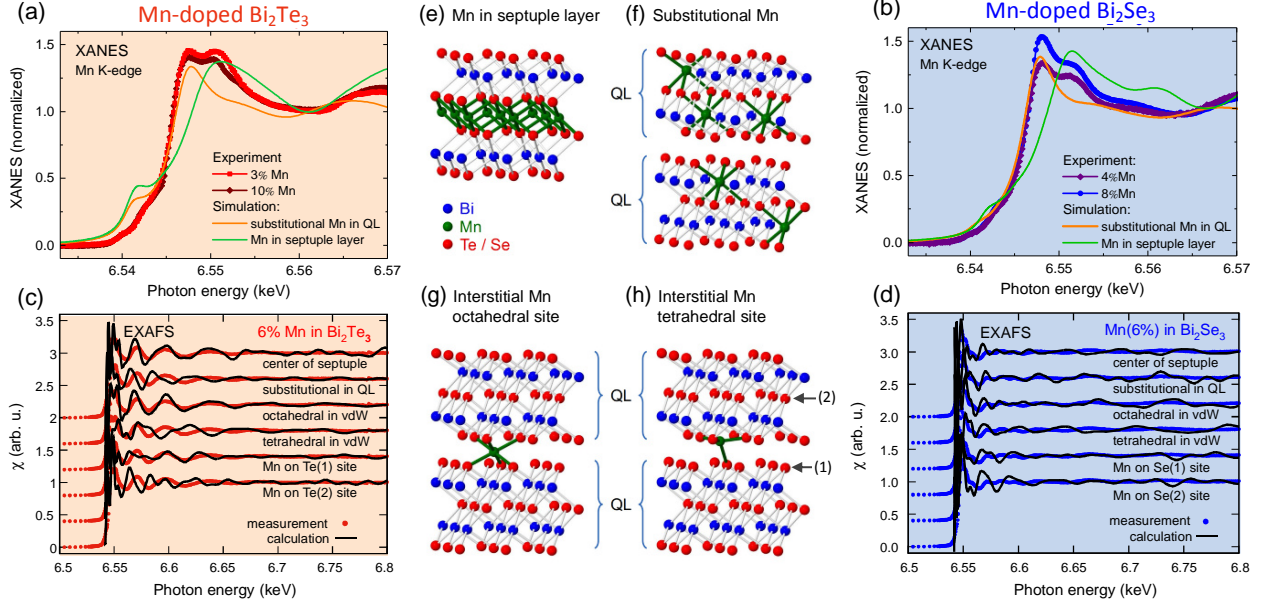
FIG. 4: **Spectroscopic determination of the Mn incorporation sites in Bi_2Te_3 and Bi_2Se_3** derived from x-ray absorption spectroscopy (XANES, EXAFS) at the Mn K-edge. The symbols represent the experimental spectra, the solid lines the simulation performed for different incorporation sites including substitutional Mn on Bi sites in quintuple layers, Mn in the center of septuple layers, as well as interstitial Mn in the van der Waals gaps as shown in (e-h). The two contributions seen in the XANES spectra (a,b) are associated with substitutional Mn sites and Mn in the center of the septuple layers, having a higher weight in Bi_2Te_3 than in Bi_2Se_3. The comparison of the EXAFS data (red lines in (c,d)) recorded for 6% Mn to the simulations (green lines) shows best agreement for Mn in the center of the septuple layers in Bi_2Te_3. EXAFS oscillations are less pronounced in Bi_2Se_3 indicating a more pronounced distribution of Mn over the different lattice sites for all Mn concentrations (see Supplementary Information).
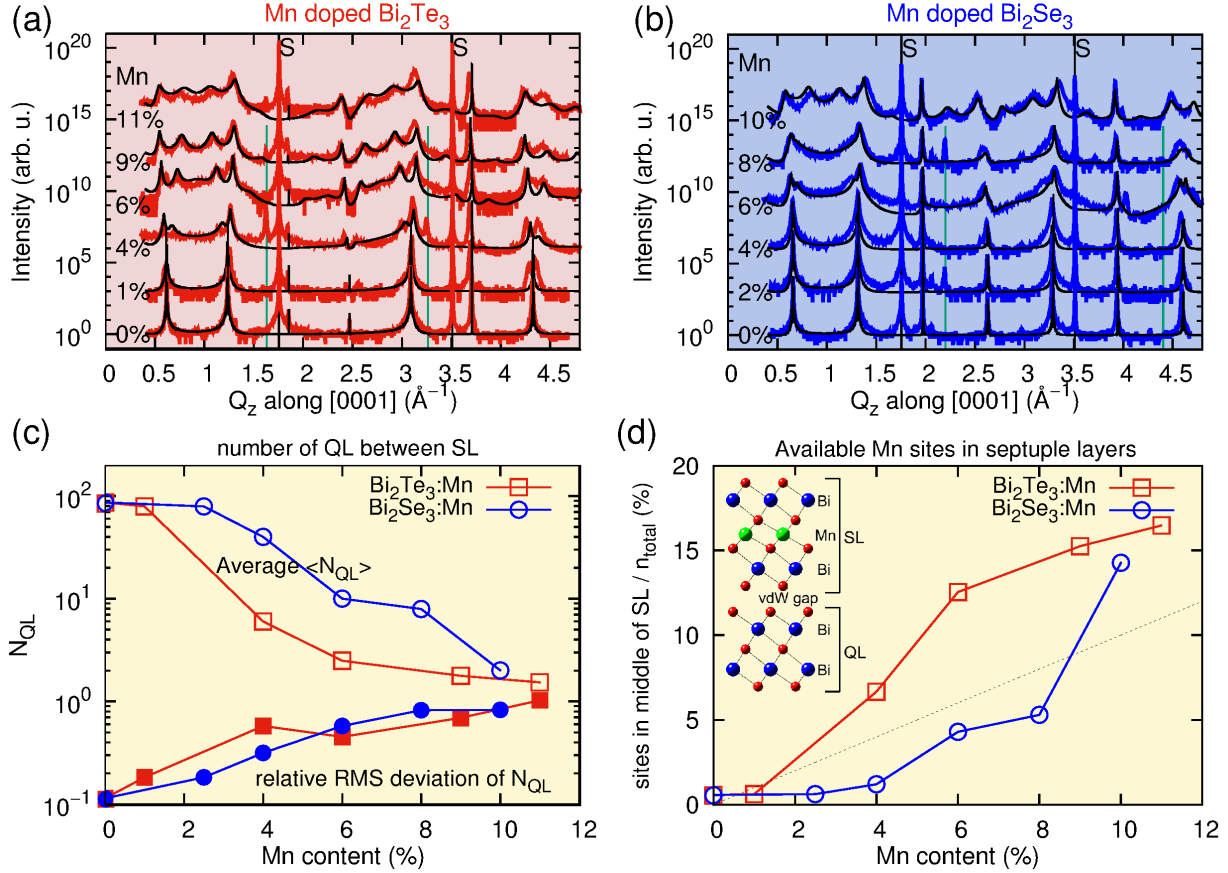
FIG. 5: **X-ray diffraction analysis of the septuple/quintuple heterostructures** formed in Bi_2Te_3 and Bi_2Se_3 upon Mn doping as a function of Mn concentration ranging from 0 to 11%. The measured diffraction spectra (red and blue lines in (a,b)) are fitted using a random stacking paracrystal model consisting of a statistically varying alternation of Bi_2X_3 quintuple and Bi_2MnX_4 septuple layers as described in the Supplementary Information, providing an excellent fit (black lines) of the experimental data for both the telluride and selenide system. The average number of quintuples $\langle N_{QL} \rangle$ between subsequent septuples and the root mean square (RMS) width of the random distribution derived from the fit is plotted in (c) versus Mn content (open, respectively, full symbols). A smaller average distance $\langle N_{QL} \rangle$, i.e., higher concentrations of septuples, is found for Bi_2Te_3 as compared to Bi_2Se_3. The number of available Mn sites in the center of the septuple layers relative to the total number n_{tot} of (Bi and Mn) atoms is shown in (d) versus nominal Mn content. The number expected for unity occupancy is indicated by the dashed line. Experimental points below the line indicate that a significant fraction of Mn atoms resides in other lattice sites. This applies to Bi_2Se_3 but not to Bi_2Te_3.